High-Temperature Performance of Alumina–Zirconia Composite Coatings Containing Amorphous Phases

Fariba Tarasi, Mamoun Medraj, Ali Dolatabadi, Jorg Oberste-Berghaus, and Christian Moreau*

Amorphous phases are commonly found in nanostructured plasma-sprayed coatings. Nonetheless, the role of these phases in the resulting coatings' properties has remained uninvestigated until now. In the present work, pseudo-eutectic coatings—based on alumina and 8 wt% yttria-stabilized zirconia (YSZ)—containing amorphous phases are produced using a suspension-plasma-spray process. These composite materials are a potential choice for thermal-barrier coating applications. The role of the amorphous phase on the performance of the coatings is investigated before and after heat treatment. Results show that, although the amorphous phases in untreated coatings reduce the thermal conductivity, they impair the mechanical properties. However, treatment above the crystallization temperature leads to better mechanical properties as well as enhanced high-temperature stability of the resulting nanostructure. Moreover, the role of alumina as a stabilizer of high-temperature YSZ phases (tetragonal and cubic) is confirmed and the high-temperature phase stability of the alumina–YSZ composite is demonstrated. The amorphous phases are found to crystallize into their corresponding high-temperature stable phases; i. e., α-alumina and tetragonal zirconia.

1. Introduction

Alumina–yttria-stabilized zirconia (alumina–YSZ) composite coatings are considered to be potential materials for thermal-barrier coating (TBC) applications.[1] As TBCs are used at high temperature, investigation of their as-coated characteristics may be insufficient for evaluating their effectiveness at service.[2] Indeed, during the first service operation, such untreated coatings and their microstructural features (porosity, crack, intersplat bonds, etc.) may undergo many changes. Moreover, amorphous-phase formation is an interesting aspect of the thermal-spray deposition of composite materials. It involves several components that retard crystallization during rapid cooling, and results in the formation of noncrystalline structures. It is now well known that eutectic systems are more likely to form amorphous phases than other compositions. Consequently, in the plasma spray deposition of the pseudo-eutectic alumina–YSZ composite, extensive amorphous-phase formation is expected. In fact, there are many reports of amorphous phases in alumina–YSZ composite coatings.[3–6] Upon exposure to high service temperature, these phases, like other structural features of the coatings, undertake changes that can, in turn, induce important variations in the properties of the deposited materials.

YSZ,[7,8] alumina,[3–10] and their composites (alumina–zirconia)[6,11–13] have been extensively investigated in terms of their crystalline and microstructural changes upon heat treatment, in addition to thermal cycling.[7] Sodeoka et al.[14] studied coatings with 50/50 volume ratio of alumina/3YSZ, and found that after 30 min at 1000 °C, crystallization of the amorphous phase was complete. However, no further phase transformation for γ-alumina and tetrahedral zirconia takes place even after 100 h at 1500 °C. In contrast, Chen et al.[8] observed the phase transformation of plasma-sprayed crystalline γ-alumina into α-alumina in half an hour at 1200 °C. Moreover, Damani et al.[10] reported the same phase transformation after heating at 1180 °C for 12 h. Nazeri et al.[13] reported the appearance of a crystalline cubic phase of zirconia at 600 °C in fully amorphous alumina/pure zirconia composites deposited by a sol-gel process. Nevertheless, for treatments below 1100 °C (which was the maximum temperature in this experiment) no crystalline alumina showed up, and the transformation from cubic to monoclinic phase started at 900 °C (noticing that the zirconia was not stabilized). In part of their research, Kirsch et al.[15] studied the performance of amorphous alumina shell over zirconia nanopowders. The powders were heated and the structural changes were monitored by using in situ X-ray diffraction (XRD). When the powder consisted of amorphous zirconia within the amorphous alumina shell, the crystallization of cubic zirconia started at 700 °C; the transformation to tetragonal was reported to be at 950 °C, while the monoclinic phase appeared at 1100 °C. Nevertheless, since the maximum temperature in this study was 1100 °C, the crystallization of alumina did not occur. On the other hand, starting with the tetragonal crystalline zirconia powder in the same shell of amorphous alumina, the only observed transformation was the γ-alumina crystalline-phase formation from the amorphous shell; no phase change in the zirconia was detected. In contrast, Kim et al.[6] reported

Dr. F. Tarasi, Dr. M. Medraj, Dr. A. Dolatabadi
Concordia University
Montreal, Quebec, Canada
E-mail: mmedraj@encs.concordia.ca
Dr. J. Oberste-Berghaus, Dr. C. Moreau
National Research Council Canada—Industrial Material Institute (NRC-IMI)
Boucherville, Quebec, Canada

DOI: 10.1002/adfm.201100471

the simultaneous crystallization of alumina and zirconia in Al_2O_3/2.3 wt% TiO_2-stabilized zirconia at around 945 °C.

Few of these investigations share the same transformation temperatures. No explanations have been put forward regarding possible reasons for these discrepancies in observed transformation temperatures, although Kim et al. in 1999[6] and Kirsch in 2004[15] did suggest that the apparent contradictions in the literature about the crystallization temperature of the amorphous phase in alumina–zirconia may be due to the varying amounts of this phase in the different structures studied. Nonetheless, no effort has since been made to investigate whether the amorphous phase affects the crystallization temperature, and whether this can affect other transformation temperatures and possibly the resulting crystal structures and their properties.

The objective of this study was to investigate the influence of the amount of the amorphous phases in plasma-sprayed coatings on the crystallization and phase-transformation temperatures as well as on the resulting crystalline structures. In addition, certain mechanical properties (hardness and erosion resistance) and the thermal conductivity of the composite coating were studied before and after heat treatment to investigate the role of the amorphous phases on the evolution of these properties upon exposure of the coatings to high temperatures.

2. Results and Discussion

2.1. Transformation Temperature and Amorphous Content

One of the aims of this research is to address the effect of the amorphous-phase content on the crystallization, and the consequent transformation temperatures in the composite coatings. **Figure 1** represents the two major transformation temperatures versus crystallization peak area from differential scanning calorimetry (DSC) measurements (representing the amorphous content). The transformations observed on heating the alumina–8 wt% YSZ composite coatings include crystallization and a γ- to α-alumina phase transformation. These transformations were identified based on XRD measurements of the heat-treated samples, as discussed in Section 2.2.

The crystallization temperature in Figure 1 varies from 951 to 956 °C, while the crystallization peak area ranges from 2 to 152 units, which corresponds to a 10 to 64% amorphous index. Figure 1 shows that the crystallization temperature is not affected by the amorphous-phase content. This observation contradicts the proposition of Kim et al.[6] regarding the probable influence of the amorphous content on crystallization temperature in this composite, and that the amount of this phase is the source of discrepancy in different reports.[8,10,13,15] In these reports, the composites were produced with various processes and impurity contents. Therefore, the source of the differences in crystallization temperature may be the different production processes and/or the impurities. Meanwhile, in the same range of amorphous content, the transformation temperature of γ- to α-alumina changes between 1258 and 1310 °C. Although this is not a negligible change, a dependence of transformation temperature on the amount of amorphous phase is not apparent.

2.2. Crystal-Structure Changes after Heat Treatment

Heat treatment at 1000 °C for 10 h of the highly crystalline coatings caused almost no crystallographic changes. In amorphous-phase-containing coatings with 35 and 53% amorphous indexes, however, a clear reduction in amorphous humps could be observed, although the humps did not fully disappear after 10 h. Nonetheless, the DSC results support the fact that completion of the crystallization process takes place at about 950 °C. Therefore, the remaining humps can be mainly attributed to nanograins, which are the dominant structure, especially after the crystallization.

As shown in **Figure 2**a, the initial crystalline structure in the highly amorphous sample (with about 64% amorphous index)

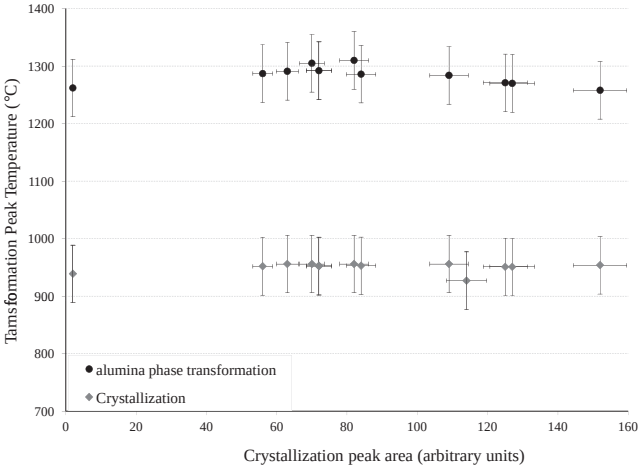

Figure 1. Transformation temperature versus crystallization peak area in DSC measurements; neither crystallization temperature nor the γ- to α-alumina transformation temperature is affected by the amorphous content.

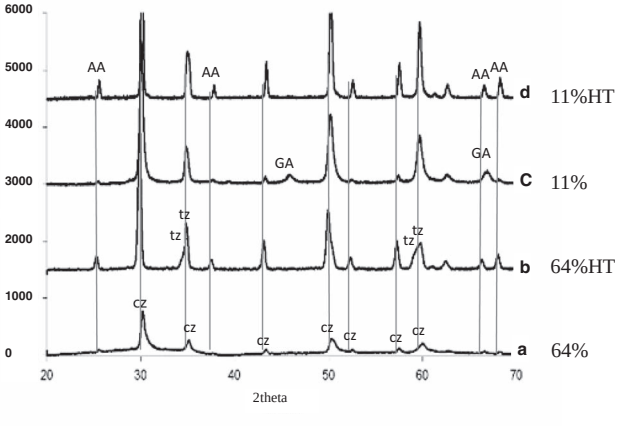

Figure 2. XRD of the highly crystalline and highly amorphous coatings before and after heat treatment at 1300 °C for 24 h: a) the coating with 64% amorphous index shows clear amorphous/nanocrystalline humps, b) 64% amorphous index coating after heat treatment, c) coating with 11% amorphous index, d) coating with 11% amorphous index; after heat treatment the hump in pattern a is visible.

consists of α-alumina and cubic zirconia. The presence of some tetragonal pattern similar to cubic phase cannot be ruled out. The highly crystalline structure in Figure 2c with about 11% amorphous index is composed of both α- and γ-alumina and cubic zirconia in untreated condition. Comparison of this pattern with that of the coatings heat-treated at 1300 °C for 24 h, shown in Figure 2b and d, suggests that in both cases, α-alumina is the dominant phase. The difference is in the YSZ dominant phase after this heat treatment, which in the case of the highly amorphous structure (Figure 2c) presents some tetragonal structure (revealed by peak splitting at 2θ between 34–35° and 59–60°). This suggests that the amorphous phase has crystallized in the form of tetragonal zirconia. This happens simultaneously with release of the dissolved alumina, which stabilizes the high-temperature cubic phase. In contrast, in the highly crystalline coating after the same heat treatment in Figure 2d, the metastable cubic YSZ is still the dominant phase after heat treatment at 1300 °C for 24 hours.

Further heat treatment at 1500 °C for 5 h was performed to investigate the possibility of monoclinic zirconia-phase formation. The XRD results showed that, apart from some grain growth during this heat treatment, traces of the monoclinic phase of zirconia were not found. Conversely, formation of monoclinic in 8YSZ (8 mol% equal to 13 wt% YSZ) was observed at 1400 °C.[16] This suggests that the very-high-temperature stability of the composite against martensitic transformation of tetragonal to monoclinic zirconia is due to the added stabilizing effect of alumina. Like the highly amorphous coatings, the highly crystalline coating shows high stability of the cubic solid solution of YSZ, even at temperatures as high as 1500 °C. These results support the role of alumina as a stabilizer through extended solubility in zirconia.

2.3. Microstructural Changes after Heat Treatment

The microstructures of the coatings after heat treatments of 1000 °C/ 10 h, 1300 °C/ 24 h, and 1500 °C/ 5 h were investigated. In **Figure 3**, the microstructures of the untreated coatings with high amorphous content (which appeared as extensive gray areas in Figure 3a) and coatings with low amorphous content (with distinctive black and white regions in Figure 3b) are shown. Treatment for 10 hours at 1000 °C did not produce any visible changes in the microstructures (not included in Figure 3). However, after treatment at 1300 °C for 24 h, the two coatings can be compared (Figure 3c and d); some spotty areas have formed in the location of previously gray regions due to the precipitation of alumina and zirconia as a result of crystallization of the amorphous phases. Accordingly, more precipitates can clearly be seen in the case of the highly amorphous structure (Figure 3c). These precipitates are typically at least 50 nm. Treatment at higher temperatures (1500 °C for 5 h), as shown in Figure 3e and f, shows the growth of precipitates as well as some spheroidization of the splats in the form of round corners and thickened splats. As a result, the microstructures of the two types of coatings with high and low amorphous content tend to show more similarities after this heat treatment.

2.4. Grain Sizes after Heat Treatment

The grain sizes of the crystalline phases were measured after heat treatment and compared with the untreated samples. **Figure 4** shows the grain sizes of different phases present before and after heat treatment. In this figure, the coatings with high crystallinity (less than 11% amorphous index), highly amorphous (45% amorphous index) and intermediate amorphous content coatings (23% amorphous index) are compared.

Figure 4a, b, and c show that, upon heat treatment of highly crystalline coatings, the average grain size increases for all phases including α-alumina, γ-alumina, and cubic or tetragonal zirconia. In contrast, upon heat treatment of highly amorphous coatings, the average grain sizes of α-alumina (Figure 4a) and zirconia (Figure 4c) decrease. The γ-alumina (Figure 4b), initially absent in this coating, appears with the smallest grain size by crystallization from the amorphous phase. In addition, the intermediate amorphous coating shows a slight grain-size reduction in all phases.

Since the initial crystalline grains grow on heat treatment, the reduced average grain size observed in highly amorphous coatings is attributed to crystallization of the amorphous regions. This means that the crystallized grains from the amorphous phase form in much smaller sizes than those formed during plasma-spray deposition (which represents rapid solidification). Thus, despite grain growth of crystalline grains, the average grain size after crystallization decreases relative to the untreated state, and this decrease is linked to the amorphous content.

It is known that the grain size of the crystalline structure grows upon heating. On the other hand, crystallization of the amorphous phase as a solid-state transformation provides a shorter free path and mobility for atomic diffusion than in the case of solidification from the liquid state. This can justify the observed smaller grain size of γ-alumina from crystallization (in 45% amorphous index coating) than that formed in untreated coatings (in the range of cooling rates provided in this experiment). The final grain size on crystallization is a compromise between two phenomena: the growth of the crystalline grains and the formation of nanosized crystalline grains from the amorphous phase (with smaller grain size than the untreated grains). As a result, a higher amorphous proportion of the structure leads to smaller average grain size on crystallization from heat treatment. Thus, transformation from the amorphous phase may be an effective way to achieve nanostructured coatings.

Further heat treatment at 1300 °C for 24 h resulted in grain growth of both crystalline and highly amorphous coatings, with a considerably higher growth rate in the crystalline coating. The grain size of the untreated and the heat treated samples are summarized in **Table 1**. This table shows that in highly crystalline coatings, the grain sizes of zirconia and α-alumina starting at 23 and 34 nm, respectively, grow to the extent that the XRD evaluation method, with its accuracy limited to a maximum grain size of about 100 nm,[17] cannot yield the grain size. These cases are marked as ">100 nm" in Table 1. In addition γ-alumina, initially smaller than the two other phases, has entirely transformed into α-alumina. On the other hand, the grain growth in the highly amorphous structure is clearly lower than in the highly crystalline coating. As Table 1 presents,

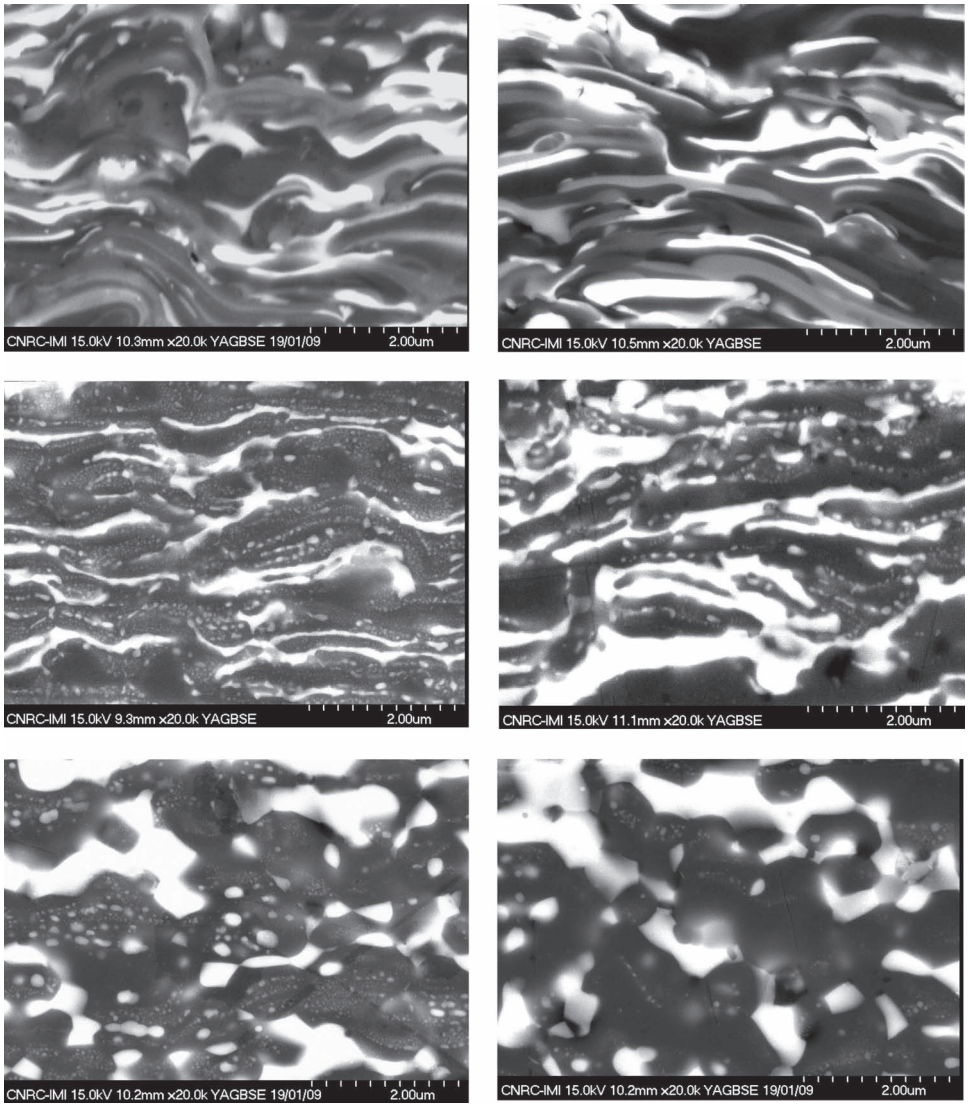

Figure 3. Microstructure of: a) untreated highly amorphous coating, b) untreated less amorphous coating, c) highly amorphous coating heat treated at 1300 °C/ 24 h, d) less amorphous coating heat treated at 1300 °C/ 24 h, e) highly amorphous coating after 1500 °C/ 5 h, f) less amorphous coating after 1500 °C/ 5 h.

zirconia grew from 19 to 40 nm, and γ-alumina was transformed into α-alumina (initially absent in the coatings), which appears at 53 nm grain size.

After heat treatment at 1500 °C for 5 h, the grain size of the crystalline phases (i.e., zirconia and α-alumina) cannot be determined due to excessive grain growth, as discussed above. However, it is clear that the grain size is larger than 100 nm.

2.5. Mechanical Properties Before and After Treatment at 1000 °C for 10 Hours

2.5.1. Hardness

Microhardness measurements on the coatings with various amounts of amorphous phase before and after heat treatment are summarized in **Figure 5**. It is apparent that the more highly amorphous coatings are of lower hardness than the crystalline structures. However, the mechanical properties such as hardness can also vary greatly with microstructural characteristics (porosity, intersplat bounding, structural integrity, etc). Upon heat treatment, the highly crystalline structure shows some decrease in hardness due to observed grain growth while crystallization of the amorphous phase into rather smaller grains enhances the hardness of the highly amorphous coatings.

Comparison of the increase in the hardness of the samples with 23 and 45% amorphous indexes shows that the increase in the hardness is greater for more highly amorphous samples. Again this is likely to be due to the greater decrease in mean grain size at higher amorphous contents. Eventually, after heat treatment, the hardness for all coatings with any amorphous content approaches a similar value, as shown in Figure 5.

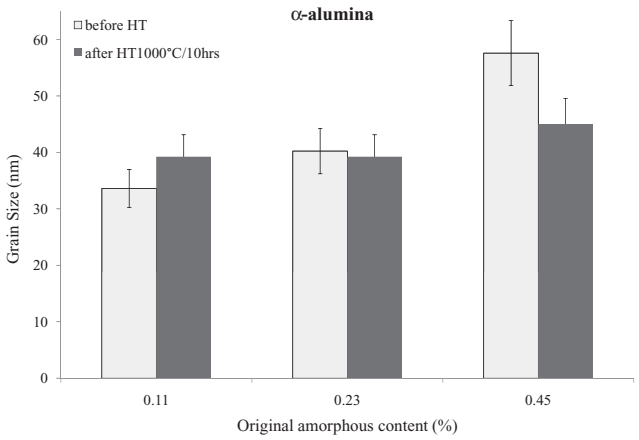

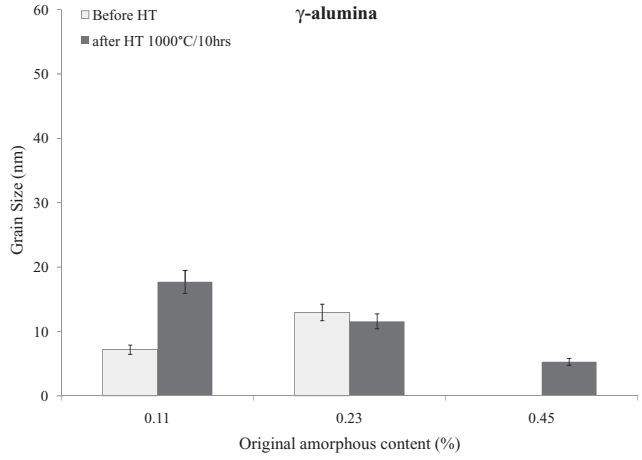

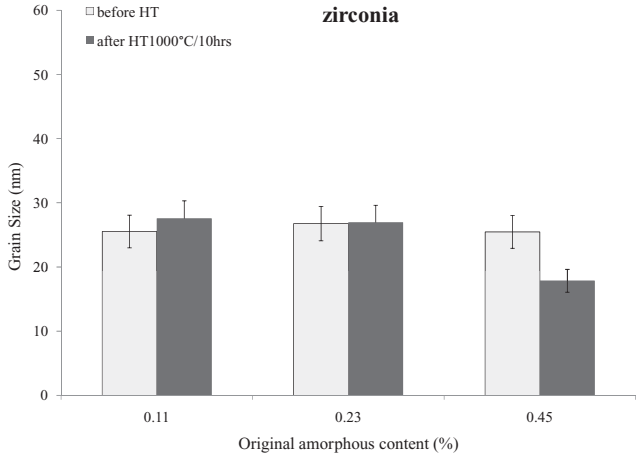

Figure 4. The role of amorphous content on grain-size changes during heat treatment for a) α-alumina, b) γ-alumina, and c) zirconia.

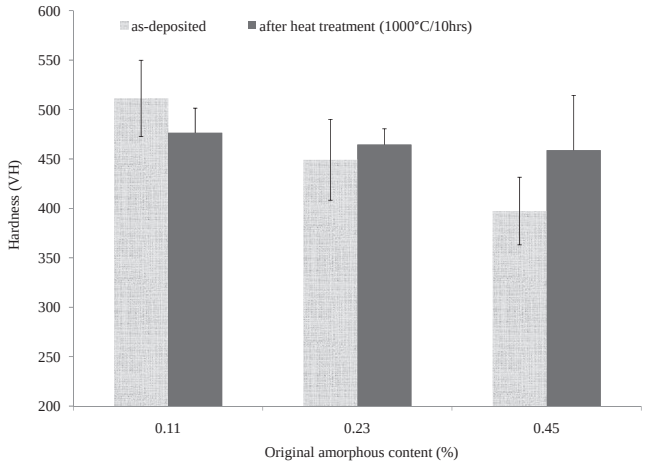

Figure 5. Hardness measures before and after heat treatment for various amorphous coatings.

2.5.2. Erosion

The erosion rate of the two coatings with 36 and 53% amorphous indexes are shown in **Figure 6**. The more highly amorphous coating undergoes a larger erosion loss. This is consistent with the hardness results, again showing that the more highly amorphous coatings are softer. Evans et al.[18] suggested that, at high obliquity of the impinging erodent particles, as in the current work, the softer ceramic phase behaves like a metal, in which the material erodes more rapidly at lower hardness.

After heat treatment at 1000 °C for 10 h, the erosion rate of the coatings has increased. This can be attributed to the sintering of the columnar grains in the structure. **Figure 7**a and b shows the fracture surfaces of such a coating before and after the heat treatment. In Figure 7a, the columnar grains that formed in the coating during suspension plasma spraying (SPS) of the alumina–YSZ composite can be seen. Figure 7b shows the same sample after heat treatment. In this figure, the annihilation of the columnar grains and the spaces between them is clear. Densification of the columnar grains in YSZ is suggested to favor rapid growth of the lateral cracks and material removal during particle impingement in erosion tests.[18]

The monolithic structure of 8 wt% YSZ, however, shows much higher erosion resistance than the composite coating of alumina–YSZ. The dense uniform structure of the 8 wt% YSZ coating, with considerably fewer structural defects, provides it with a superior erosion resistance. This is in contrast with the composite coating, in which more reduction in erosion resistance was observed after 1000 °C for 10 h. This improvement in the 8 wt% YSZ can be attributed to the ceramic densification arising from elimination of porosities and interlamellar cracks due to sintering,[19] as denser ceramics are known to be of

Table 1. Role of amorphous content on grain growth during heat treatment.

	Untreated coating			After heat treatment at 1300 °C/ 24 h		
Amorphous index [%]	α-alumina [nm]	γ-alumina [nm]	zirconia [nm]	α-alumina [nm]	γ-alumina [nm]	zirconia [nm]
11	34	13	23	>100	–	>100
46	–	9	19	53	–	40

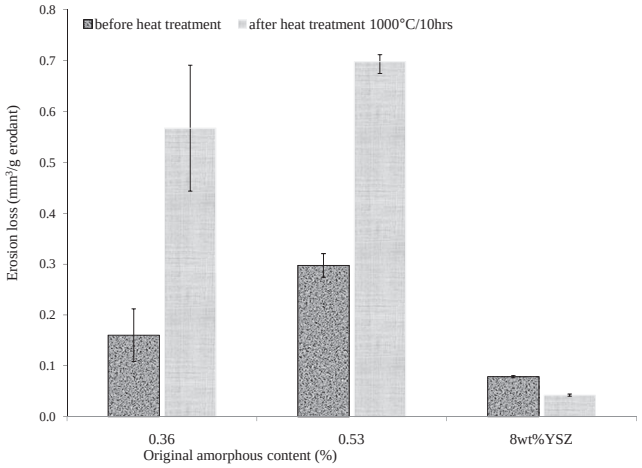

Figure 6. Erosion losses in two different amorphous coatings before and after heat treatment at 1000 °C/ 10 h; and comparison with YSZ coating with the same process.

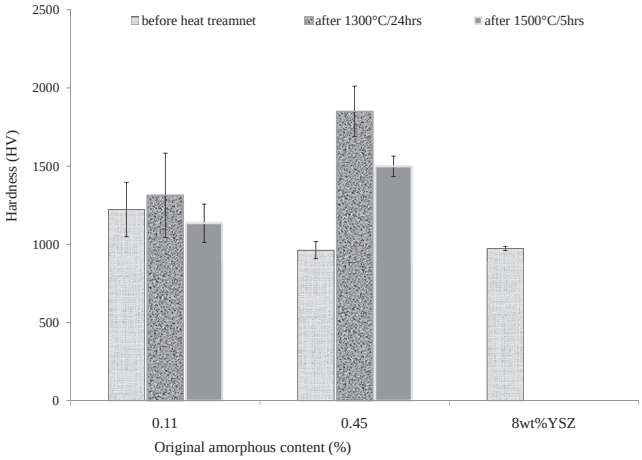

Figure 8. Comparison of the hardness variation with heat treatment between two samples with low and high amorphous content and their comparison with the 8 wt% YSZ.

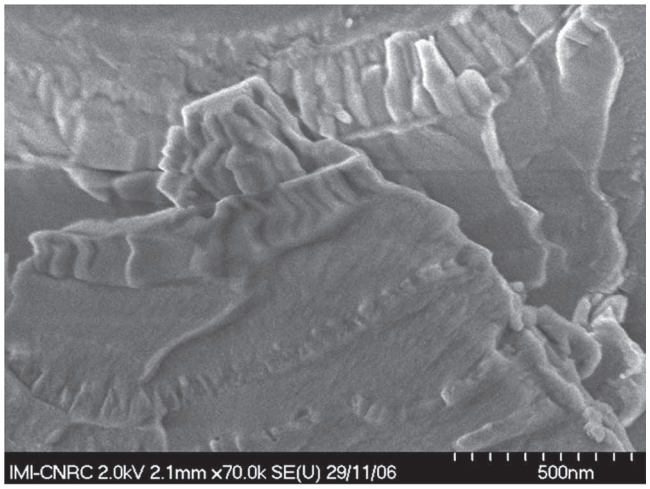

Figure 7. Fracture surface of alumina–YSZ coating deposited by SPS: a) before, and b) after heat treatment at 1000 °C for 10 h, showing annihilation of columns and sintering of the structure.

higher erosion resistance.[20] Apparently the effect of sintering on the erosion resistance of the composite coating is the opposite to that seen on the monolithic coating, in which sintering annihilates the columnar grains, resulting in better erosion resistance. This observation requires further investigation.

2.6. Mechanical Properties Before and After Treatment at 1300 °C for 24 Hours, and at 1500 °C for 5 Hours

As shown in **Figure 8**, in the highly crystalline structure the hardness is initially higher than in the highly amorphous structure. After heat treatment at 1300 °C for 24 h, the hardness remains almost unchanged in the crystalline structure, while in the highly amorphous coating it increases considerably due to the presence of precipitates (shown in Figure 3c and d) that have enlarged during heat treatment to an effective size, which improves the mechanical properties.

After treatment at 1500 °C for 5 h, the hardness decreases due to grain growth and to overaging, which causes additional growth of the precipitate (shown in Figure 3e and f). Yet, this hardness is greater than that of the untreated crystalline coating. Thus, the amorphous phase initially lowers the hardness but upon heat treatment it increases the hardness due to a smaller average grain size, as well as to sintering and densification. The hardness of 8 wt% YSZ is shown to be lower than that of the alumina–8 wt% YSZ composite.

2.7. Thermal Conductivity Before and After Heat Treatment

Figure 9 represents the relationship between thermal conductivity of the coatings before and after heat treatment, while the crystallization peak area represents the original amount of amorphous phases in the coating before heat treatment. It can be seen that before heat treatment, the thermal conductivity

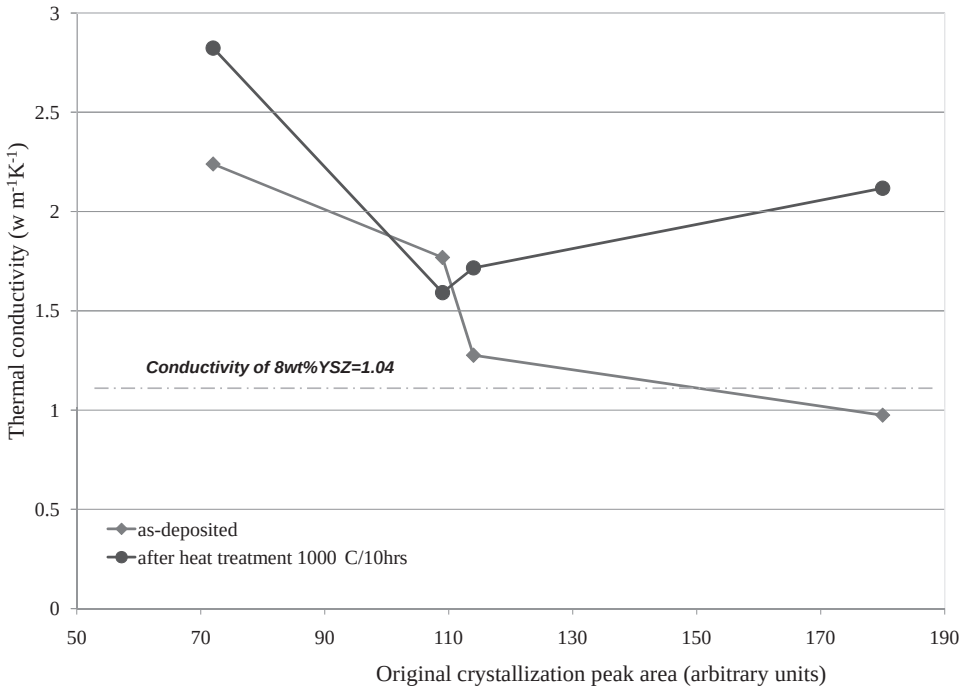

Figure 9. Thermal conductivity changes before and after heat treatment at 1000 °C/ 10 h for coatings with various amorphous contents.

decreases as the proportion of amorphous phase increases. According to the literature,[21] other than radiation, there are two mechanisms of thermal conduction in solids. The first is electron transfer (mostly active in metals), and the second is phonon transfer in nonmetallic crystalline solids like ceramics. This means that in the absence of readily moving electrons to transfer the thermal energy, the energy is transferred by crystallite vibration. In amorphous-containing ceramics the second mechanism for heat transfer is also impaired due to the reduced mean free path of phonons in the amorphous phase. Heat treatment is thus expected to give rise to decreased thermal conductivity by increasing the proportion of amorphous phase.

Upon heat treatment at 1000 °C for 10 h, crystallization can reactivate the photon transfer mechanism and increase the thermal conductivity. As can be seen in Figure 9, the heat-treated samples (except one) present higher thermal conductivity than the initial coatings. In addition, in the heat-treated coatings with high amorphous content (last three points), the thermal conductivity increases with the amorphous content. This can be attributed to the formation of higher amounts of tetragonal structure in the highly amorphous coatings, as discussed earlier, compared with the more crystalline coating, which mainly consists of cubic zirconia with lower thermal conductivity.[22]

In a closer investigation of the microstructure of the sample that showed lower thermal conductivity than before heat treatment, a high number of tiny horizontal cracks can be observed in the coating. The heat treatment opens these cracks and reduces the thermal conductivity. Since increasing the amorphous content diminishes the thermal conductivity, coatings with high amorphous content (as in the last data point in Figure 9) yield low thermal conductivity (comparable to that of 8 wt% YSZ).

3. Conclusion

The amount of amorphous phase does not affect the crystallization temperature and the γ- to α-alumina transformation temperature. However, the amorphous phase is an effective source of nanocrystalline structure on heat treatment, with smaller and more stable grain sizes than can be produced by plasma spray. Thus, crystallization from amorphous phase is a promising method for producing nanostructured coatings.

In terms of mechanical properties, the pseudoeutectic alumina–YSZ composite shows superior hardness over the presently used 8 wt% YSZ TBC deposited by the same process. The coating is, however, inferior in erosion resistance to the 8 wt% YSZ.

The hardness of the amorphous-phase-containing coatings is initially lower than that of the crystalline coating. Crystallization results in similar hardness in both coatings. However, during heat treatment at 1300 °C, precipitation of zirconia in the alumina matrix results in greater hardness than that of the crystalline coating. However, after treatment at higher temperature (1500 °C) the two materials show similar hardness. In addition, erosion loss in the highly amorphous coating is greater than in the crystalline coating.

Higher amorphous content reduces the thermal conductivity, whereas crystallization increases it. In addition, coatings with higher amorphous content experience a greater increase in thermal conductivity after crystallization heat treatment due to crystallization of amorphous phase into tetragonal rather than cubic zirconia.

The pseudoeutectic alumina–YSZ composite shows high thermal stability, which prevents the formation of monoclinic zirconia. In addition, a solid solution of cubic YSZ with alumina

presents high thermal stability even at temperatures as high as 1500 °C.

4. Experimental Section

Coating samples of pseudoeutectic (60/ 40 wt%) composition of alumina–8 wt% YSZ were sprayed using SPS, which is a modification of the conventional plasma spray process in which a liquid carrier is used to transport nano or several-micron-sized powder feed to the injection nozzle. The alumina–YSZ powders are axially injected into the plasma flame in an Axial III plasma torch (Northwest Mettech, North Vancouver, Canada). Nano- and microsized powders of alumina and YSZ are mixed and deposited under various spray conditions. 8 wt% YSZ coatings were also prepared as the reference material, by the same method. Nanopowders included 13 wt% YSZ (Inframat, Farmington, CT, USA) with proportional weight of 5 wt% YSZ to produce 8 wt% YSZ and alumina nanopowder (Nanostructured & Amorphous Materials, Houston, TX, USA). The particle size of this mixture was between 20 and 60 nm. Micron powders included 13 wt% YSZ (Unitec Ceramics, Stanford, England) with a nominal size of 1 μm, combined with the proportional amount of 5 wt% YSZ (Tosoh TZ-3YS, Tokyo, Japan) to produce 8 wt% YSZ and mixed with alumina powder (Malakoff, TX, USA) with a nominal size of 1.4 μm in a weight ratio of 60 alumina/40 YSZ. Nano and micron powders were suspended into ethanol, with solid contents of 10 and 30 wt%. To stabilize the suspensions and prevent settling of the powder particles, polyethylene-imine (PEI) (MW 25,000 Alfa Aesar, Ward Hill, MA, USA) and nitric acid (both 10% aqueous solutions) were used as dispersants. PEI (18 mL) and nitric acid (9 mL) were added for each 150 g of suspension. These proportions were selected based on trial and error to get the most stable suspensions. In addition, suspensions were ball milled for more than 24 h at 120 rpm to avoid large aggregates. Magnetic mixing in the container during the spray process was also used to keep the distribution of solid particles in the suspension uniform. The suspensions were then injected into the plasma torch with a feed rate between 1.3 and 1.8 kg h^{-1}. The spray distance was 50 mm and the substrate temperature was maintained at a maximum of 400 °C. Substrates for erosion test samples were large (25 × 35 × 125 mm), while the rest of the substrates were smaller (25 × 25 × 5 mm). The plasma powers used were in the range of 50 to 120 kW; total plasma gas flows were in the range between 245 and 275 standard L min^{-1}. These variables were changed to provide coatings with various amounts of amorphous phase. More specific details of the production procedures and how the variables could affect the amorphous contents can be found elsewhere.[23] As a result, alumina–8 wt% YSZ composite samples of similar composition, but with amorphous indexes[23] ranging from 0–64% became available.

The coatings were ranked according to their amorphous content using two methods. One was based on their amorphous index, which is the ratio of the amorphous hump areas to the total area of the crystalline peaks and humps in XRD patterns in the 2θ range between 20 and 90 ° (as explained elsewhere[23,24]). The other method of comparing amorphous phases is according to the crystallization peak areas in the DSC curves.

XRD patterns were obtained using Bruker D8-Discovery diffractometer (Bruker AXS, Madison, WI, USA), and DSC graphs were produced by the TG96 (SETARAM, Caluire, France) apparatus. In addition, microstructural studies on the cross section of the coatings were performed using a field emission-scanning electron microscope (Hitachi S4700, Blackwood, NJ, USA).

Samples were heat treated in air at 1000 °C for 10 hours, 1300 °C for 24 h, and 1500 °C for 5 h. The first and the second heat treatment temperatures were selected to be above the phase-transition temperatures for γ- to α-alumina and tetragonal to monoclinic transformations, respectively. The third heat treatment was to investigate the high temperature stability of the microstructures. Thermal conductivity and mechanical properties before and after heat treatment were compared among coatings with various amounts of amorphous phases. The roles of amorphous content on transformation temperatures were studied using the DSC curves and their transformation peaks.[25] High-temperature structural stability was investigated using XRD.

Grain sizes were measured based on the XRD peak widths and using Scherrer's formula.[17] For these calculations, the most reliable peaks (without overlapping or with minimal overlapping) for each phase were selected as follows: Planes (111) for cubic zirconia or (110) for tetragonal zirconia, both at about 2θ = 30°, (200) at about 68° for γ-alumina and (300) at about 46° for α-alumina phase. The best curve fitting using the "peak fitting" function of GRAMS software[26] was used for peak measurements (width and angle). To eliminate the machine broadening effect, Equation 1 was used to find the corrected peak width B,

$$B = \sqrt{b^2 - \beta^2} \quad (1)$$

where b is the measured peak width and β is the machine broadening as determined from the peak width of a reference LaB6 single crystal. The thermal diffusivity of the coatings was measured at room temperature using the laser flash technique.[27] In this method, a thermal pulse generated by a laser beam is applied on one face of the free-standing coating of a 7 mm square and the temperature history on the opposite side is used for calculations of thermal diffusivity through the coating thickness. The thermal conductivity is calculated using Equation 2;

$$k = \rho \,.\, C_p \,.\, \alpha \quad (2)$$

where C_p is the specific heat capacity at room temperature and constant pressure measured using calorimetric technique, based on ASTM (American Standard for Testing Materials) E1269-05 "Standard Test Method for Determining Specific Heat Capacity by Differential Scanning Calorimetry", and ρ is the density of the coating based on theoretical density and taking into account the porosity of the coatings for each sample (around 2%[28]). The slight density variations due to phase changes during heat treatment are not taken into account. Prior to measurement, the coatings were detached from the substrate using boiling hydrochloric acid (50 vol%).

The microhardness test was performed using the AB-Buehler hardness-testing apparatus (Buehler, Illinois, USA) at 300 grf for 15 s at 10 different locations with a minimum distance of three times the indent diagonal in the cross section of the coatings.

Erosion resistance was determined based on the material loss due to gas-entrained solid-particle impingement, and according to the amended ASTM standard test method G76-83 "Standard Practice for Conducting Erosion Tests by Solid Particle Impingement Using Gas Jets". In this experiment, the 100 grit alumina abrasive powder was blasted using an air flow of 10 L min^{-1}. Coatings were exposed to the particle jet at a 30° angle (instead of 90° mentioned in the standard procedure) for 30 s (instead of 10 min), spraying erodent powder (about 3.7 g min^{-1}). The shorter time was used for the sake of thinness of the coatings (a few hundred microns). Three replicates were used for each evaluation. The results were reported based on the volume loss of the coating per unit weight of applied erodent solid. The error bars are calculated from the standard deviation of the three measurements.

Acknowledgements

The authors thank NSERC for partial financial support of this work. They also thank M. Thibodeau, J.-F. Alarie, S. Bélanger, F. Belval, B. Harvey, and M. Lamontagne from the Industrial Materials Institute of the National Research Council (IMI-NRC) for their technical support. Additional appreciation goes to D. Kevorkov of Concordia University for help in analyzing the XRD results.

Received: March 2, 2011
Revised: April 21, 2011
Published online: September 15, 2011

[1] P. Ramaswamy, S. Seetharamu, K. B. R. Varma, K. J. Rao, *Compos. Sci. Technol.* **1997**, *57*, 81.
[2] L. Xie, X. Ma, E. H. Jordan, N. P. Padture, D. T. Xiao, M. Gell, *Mater. Sci. Engineering A* **2003**, *362*, 204.
[3] M. Suzuki, S. Sodeoka, T. Inoue,*Trans. Mater. Res. Soc. Jpn* **2004**, *29*, 405.
[4] M. Suzuki, T. Inoue, S. Sodeoka, *Conf. Proc. Materials Technologies (Faenza, Italy)* **2003**, 381.
[5] H. J. Kim, K. M. Lim, B. G. Seong, C. G. Park, *J. Mater. Sci.* **2001**, *36*, 49.
[6] H. J. Kim, Y. J. Kim, *J. Mater. Sci.* **1999**, *34*, 29.
[7] L. Xie, E. H. Jordan, N. P. Padture, M. Gell, *Mater. Sci. Eng. A* **2004**, *381*, 189.
[8] C. Zun, R. W. Trice, M. Besser, Y. Xiaoyun, D. Sordelet, *J. Mater. Sci.* **2004**, *39*, 4171.
[9] K. S. Ravichandran, K. An, R. E. Dutton, S. L. Semiatin, *Am. Ceram. Soc.* **1999**, *82*, 673.
[10] R. J. Damaini, P. Makroczy, *J. Eur. Ceram. Soc.* **2000**, *20*, 867.
[11] A. M. Limarga, S. Widjaja, T. H. Yip, *Surf. Coat. Technol.* **2005**, *197*, 93.
[12] G. Shanmugavelayutham, S. Yano, A. Kobayashi, *Vacuum* **2006**, *80*, 1336.
[13] A. Nazeri, S. B. Qadri, *Surf. Coat. Technol.* **1996**, *1–3*, 166.
[14] S. Sodeoka, M. Suzuki, T. Inoue, *Key Eng. Mater.* **2006**, *317–318*, 513.
[15] B. L. Kirsch, A. E. Riley, A. F. Gross, S. H. Tolbert, *Langmuir* **2004**, *20*, 11247.
[16] J. Ilavsky, J. K. Stalick, J. Wallace,*J. Therm. Spray Technol.* **2001**, *10*, 497.
[17] B. D. Cullity, *In Elements of X-Ray Diffraction*, Addison-Wesley, California **1978**.
[18] A. G. Evans, N. A. Fleck, S. Faulhaber, N. Vermaak, M. Maloney, R. Darolia, *Wear* **2006**, *260*, 886.
[19] J. Ilavsky, G. G. Long, A. J. Allen, *15th International Thermal Spray Conference (Nice, France)* **1998**, 1641.
[20] J. G. Murphy, H. W. King, P. Mayer, *Can. Ceram. Quarterly* **1987**, *56*, 21.
[21] J. P. Holman, *Heat Transfer* Mc Graw Hill, Boston, USA **2002**.
[22] R. K. Williams, J. B. Bates, R. S. Graves, D. L. McElroy, F. J. Weaver, *Int. J. Therrnophys.* **1988**, *9*, 588.
[23] F. Tarasi, *PhD Thesis*, Concordia University, Montreal, Canada **2010**.
[24] F. Tarasi, M. Medraj, A. Dolatabadi, J. Oberste-Berghaus, C. Moreau, *Surf. Coat. Technol.* **2010**, DOI: surfcoat-d-10-01852r2.
[25] F. Tarasi, M. Medraj, A. Dolatabadi, J. Oberste-Berghaus, C. Moreau, *J. Therm. Spray Technol.* **2010**, *9*, 787.
[26] Spectroscopy data processing software: GRAMS/Al 7.01, Thermo-Galactic, **2002**.
[27] A. S. Houlbert, P. Cielo, C. Moreau, M. Lamontagne,*Int. J. Therrnophys.* **1994**, *15*, 525.
[28] F. Tarasi, M. Medraj, A. Dolatabadi, J. Oberste-Berghaus, C. Moreau, *J. Therm. Spray Technol.* **2008**, *17*, 685.